The influence of Cu addition on the crystallization and magnetic properties of FeCoNbB alloys

2002 J. Phys.: Condens. Matter 14 11717

(http://iopscience.iop.org/0953-8984/14/45/313)

INSTITUTE OF PHYSICS PUBLISHING JOURNAL OF PHYSICS: CONDENSED MATTER

J. Phys.: Condens. Matter **14** (2002) 11717–11727 PII: S0953-8984(02)40192-0

The influence of Cu addition on the crystallization and magnetic properties of FeCoNbB alloys

J S Blázquez, V Franco and A Conde[1]

Departamento de Física de la Materia Condensada, ICMSE-CSIC, Universidad de Sevilla, PO Box 1065, 41080 Sevilla, Spain

E-mail: conde@us.es

Received 2 August 2002
Published 1 November 2002
Online at stacks.iop.org/JPhysCM/14/11717

Abstract

The influence of Cu addition on the crystallization process, the nanocrystalline microstructure and the magnetic properties has been studied in the $Fe_{78-x}Co_xNb_6B_{16-y}Cu_y$ ($x = 18, 39, 60$; $y = 0, 1$) alloy series. Cu addition clearly refines the nanocrystalline microstructure for the alloys with the lowest Co content, but the effect is reduced as the Co content increases. Refinement of the microstructure stabilizes the nanocrystalline microstructure by shifting the second crystallization process to higher temperatures. Cu addition mainly affects the magnetic properties for the lowest Co containing alloys. A fitting procedure of coercivity versus crystalline volume fraction is performed for these alloys in the frame of the random anisotropy model extended to two-phase systems and assuming constant magnetoelastic anisotropy.

1. Introduction

Soft magnetic nanocrystalline alloys are two-phase systems in which nano-sized ferromagnetic crystals are embedded in a residual ferromagnetic amorphous matrix with a lower Curie temperature. This microstructure can be easily achieved from the partial devitrification of a precursor amorphous alloy obtained by rapid quenching from the melt. In the first reported composition, $Fe_{73.5}Si_{13.5}B_9Nb_3Cu_1$ (Finemet) [1], small additions of Nb and Cu were found to be necessary to achieve the nanocrystalline microstructure [2]. Later, nanocrystalline microstructure was obtained in Cu-free, FeMB (M = Nb, Zr, Hf ...), alloys (Nanoperm) [3], although an addition of 1 at.% Cu does refine the grain size, improving soft magnetic properties in these compositions with respect to the Cu-free alloys [4]. New nanocrystalline alloys, the so-called Hitperm alloys (FeCoMBCu) [5], have been developed as competitive materials for high temperature soft magnetic applications. In these alloys, partial substitution of Fe by Co

[1] Author to whom any correspondence should be addressed.

enhances the Curie temperature of the residual amorphous phase, extending the temperature range of applicability.

The effect of the addition of a small amount of Cu (about 1 at.%) on the crystallization process of Finemet and Nanoperm systems is well known: Cu atoms form clusters, which enhance the heterogeneous nucleation process of the α-FeSi (in Finemet) or α-Fe (in Nanoperm), as been demonstrated from atom–probe (AP) [6, 7] and x-ray absorption (EXAFS, XANES) techniques [8–11]. However, AP results for Finemet alloys with partial Co substitution [12] show that the driving force for Cu clustering decreases as Co concentration increases in the alloy. On the other hand, recent studies on Hitperm composition $Fe_{44}Co_{44}Zr_7B_4Cu_1$ [13] show that Cu is homogeneously distributed in the as-quenched alloy and, after annealing for 60 min at 550 °C, Cu is rejected from the α'-FeCo into the residual amorphous matrix without forming clusters. However, recent 3D-AP results [14] on the Nb-containing Hitperm-type composition $Fe_{39}Co_{39}Nb_6B_{15}Cu_1$ clearly show the formation of Cu clusters (number density $\sim 3 \times 10^{24}$ m^{-3}). Therefore, it is inferred that the late transition metal (Zr, Nb ...) affects the driving force of the Cu-clustering phenomenon for alloys with high Co content.

Co substitution in Hitperm alloys also affects the magnetic properties. In fact, higher values of coercivity (H_C) can be found at room temperature for these alloys with respect to Finemet and Nanoperm, which is related to the non-negligible magnetostriction in Hitperm alloys [15]. For the nanocrystalline alloys in which magnetoelastic anisotropy is negligible, magnetocrystalline anisotropy determines the coercivity. Herzer [16] described the magnetic properties of nanocrystalline systems with negligible magnetoelastic anisotropy using the random anisotropy model in the approximation of single-phase systems. A D^6 law (where D is the grain size) for H_C was found. Lately, Hernando *et al* [17] extended the model to two-phase systems and explained several points not described by Herzer's model, specially the behaviour of coercivity for low crystalline volume fraction and its evolution with the temperature.

These models have been extensively applied to Finemet- and Nanoperm-type alloys [15]. However, a detailed study of the relationship between coercivity and crystalline volume fraction is not available for Hitperm-type alloys. The aim of this work is to study the effect of Cu addition on the microstructure, magnetic properties and crystallization process in the $Fe_{78-x}Co_xNb_6B_{16-y}Cu_y$ ($x = 60, 39, 18$; $y = 0, 1$) alloy series. The relation between microstructure and coercivity will be studied in the frame of the random anisotropy model extended to two-phase systems [17].

2. Experimental details

Amorphous ribbons, about 20 μm thick and 5 mm wide, of nominal composition $Fe_{78-x}Co_xNb_6B_{16-y}Cu_y$ ($x = 18, 39$ and 60; $y = 0, 1$) were prepared by a single-wheel melt-spinning technique. Differential scanning calorimetry (DSC) (Perkin–Elmer DSC7) was used to observe the devitrification processes. Transmission electron microscopy (TEM) (Philips CM20, 200 kV) was used to observe the microstructure of nanocrystalline samples. Room-temperature coercivity has been measured from quasistatic hysteresis loops performed on a homemade system [18]. Samples were annealed in argon atmosphere in an halogen lamp furnace.

3. Results and discussion

Previous DSC studies [19] showed that the nanocrystallization process is affected by the addition of 1 at.% of Cu for all the studied alloys in a similar way. Crystallization onset and

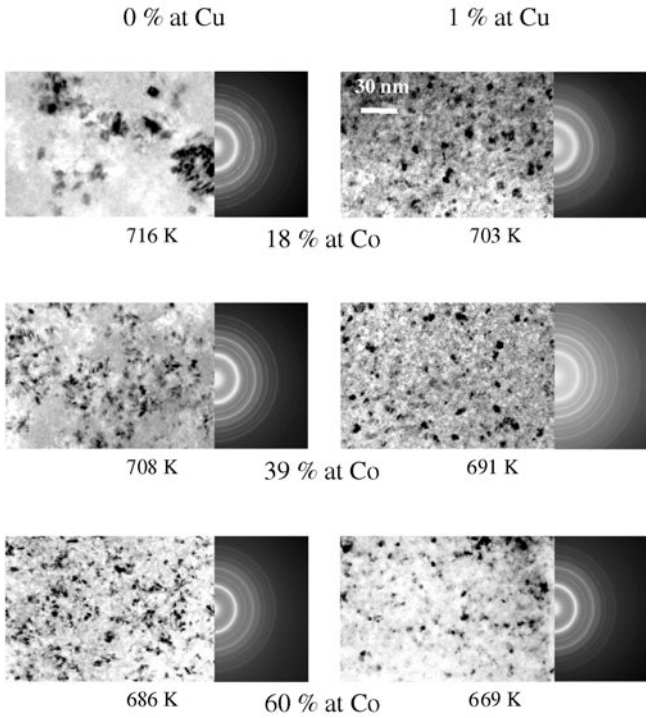

Figure 1. BF images and SAD pattern of samples of the different alloys annealed 750 min at equivalent temperatures (35 K below the crystallization onset temperature).

peak temperatures shift to lower values for the alloys with Cu, the shift of the onset temperature being ∼10–20 K larger than the shift of the peak temperature. The peak shape is smoother in the alloys with Cu: the temperature range of the transformation is 15–30% wider and the maximum transformation rate (dH/dt at the peak temperature) is 30–60% smaller in the Cu-containing alloys with respect to the corresponding Cu-free alloy. This indicates a similar effect of the Cu addition on the nanocrystallization process of the studied alloys, independent of their Co content. X-ray diffraction studies [19] showed that final crystalline volume fraction is independent of Cu addition, so the important parameter for characterization of the differences induced in the microstructure by Cu addition is the grain size.

3.1. Cu effect on the nanocrystalline microstructure

Figure 1 shows bright-field (BF) TEM images and selected area diffraction (SAD) patterns of the studied alloys for samples submitted to equivalent annealing procedures (750 min at 35 K below the crystallization onset temperature). Grain size distribution profiles for these samples are shown in figure 2. In the alloy series without Cu, the grain size decreases as the Co content increases in the alloy, whereas for Cu-containing alloys the microstructure shows similar grain sizes independently of Co content. The main difference induced by Cu addition in the microstructure of the alloys with 18 and 39 at.% of Co is a narrower grain size distribution with respect to that found for Cu-free alloys. However, in the 60 at.% Co-containing alloys, both distributions (for Cu-free and Cu-containing alloys) are similar.

These differences in the grain size exist throughout the nanocrystallization process, as can be observed in figure 3, which shows the average grain size versus annealing time for the

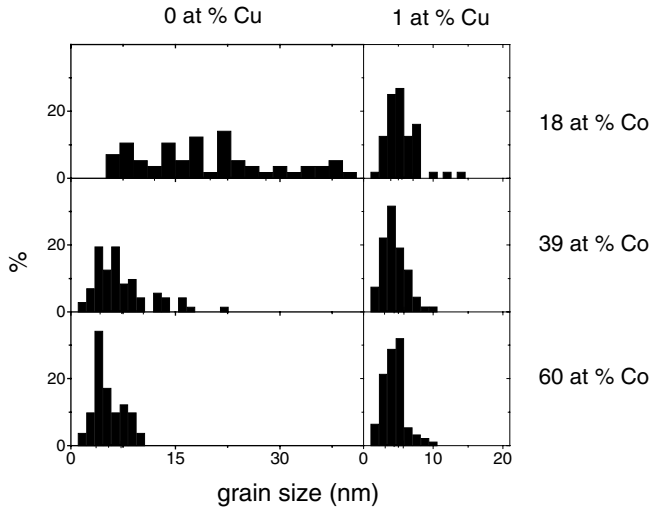

Figure 2. Mean grain size distribution for samples of the different studied alloys annealed for 750 min at equivalent temperatures (indicated in figure 1).

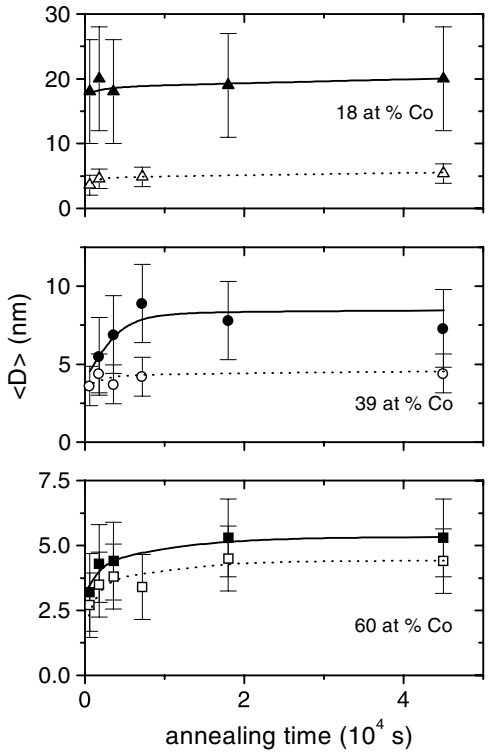

Figure 3. Grain size versus annealing time for samples of the different studied alloys annealed at equivalent temperatures (indicated in figure 1).

different studied alloys (subjected to equivalent isothermal treatments). Grain size increases abruptly for short annealing times, remaining approximately constant for longer annealing.

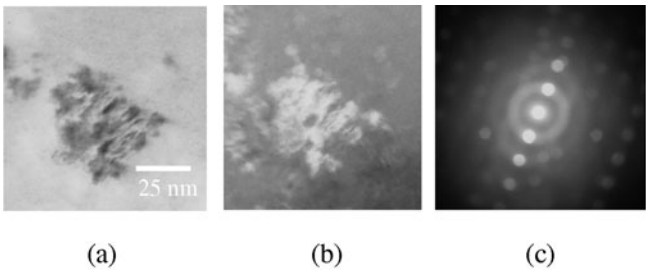

Figure 4. (a) BF image, (b) DF image and (c) Kössel–Möllensted CBED pattern of a nanocrystal for a sample of $Fe_{60}Co_{18}Nb_6B_{16}$ alloy annealed 750 min at 716 K.

Cu-containing alloys show smaller average crystal sizes than the corresponding Cu-free alloy with the same Co content for any annealing time for all the studied compositions. This difference decreases as the Co content increases in the alloy, being smaller than 1 nm for the 60 at.% Co-containing alloy.

Refinement of microstructure means a smaller grain size and implies a higher number density of crystalline nuclei provided that the crystalline volume fraction is the same. In the studied alloy series, microstructure refinement can be obtained by adding 1 at.% of Cu or increasing Co concentration. Both changes must affect the nanocrystallization by an enhancement of the nucleation process with respect to the growth process.

As reported for Nanoperm alloys [20], fcc Cu clusters and α-Fe nanocrystals have crystallographic relations indicating an epitaxial growth of the nanocrystals. These results show that Cu clusters offer a reduced surface energy for the formation of new nuclei of bcc phase on the Cu cluster surface.

In a Cu-free alloy, the surface energy of a forming nucleus might be lowered if the nucleus is close to the surface of a nanocrystal already formed and orientationally related to it, this being a growth process of these nanocrystals. For the Cu-free alloys with 18 and 39 at.% of Co, the microstructures show irregular-shaped grains, as predicted by the crystallization mechanism indicated above. The orientational relation for the large irregular nanograins (20–30 nm) of 18 at.% Co containing alloy without Cu is shown in figure 4. In this figure, the BF image, dark-field (DF) image and convergent beam electron diffraction (CBED) pattern of the same nanocrystal show that the particle is not composed by randomly orientated bcc crystals but by smaller 'nanocrystals' with the same orientation (actually, they are considered all together as only one nanocrystal in the text).

For Cu-free alloys, the number density of nanocrystals for the alloy with 18 at.% of Co is smaller than for 39 at.% Co-containing alloy (figure 1). This can be understood in terms of the composition of the nanocrystals, which are enriched in Fe and reject B and Nb to the matrix, whereas Co is homogeneous throughout the amorphous matrix and the nanocrystals [14]. Once a nucleus is formed and the nanocrystal grows, the surrounding amorphous matrix becomes poorer in Fe content, and nucleation in an isolated area (far from other nanocrystals and richer in Fe) might be energetically more advantageous than nanocrystal growth. This impoverishment in Fe might be larger as the Co concentration in the precursor alloy increases, because Fe content in the alloy is smaller. For nanocrystal compositions of $Fe_{82}Co_{18}$, $Fe_{61}Co_{39}$ and $Fe_{40}Co_{60}$, for the alloys with 18, 39 and 60 at.% Co content, respectively, the Fe concentration in the nanocrystals might increase by 37, 56 and 122% with respect to the initial amorphous concentration, respectively. This effect is associated with nanocrystallization kinetics results [21], which show slower kinetics as the Co content increases in the alloy.

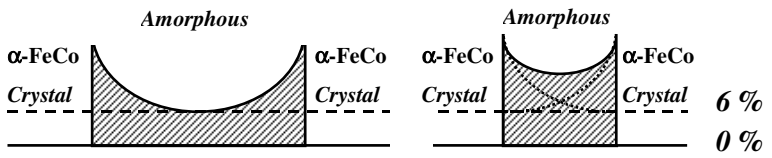

Figure 5. Schematic representation of the dependence of Nb concentration profile on the amorphous layer thickness between neighbour nanocrystals. The 6% level represents the Nb concentration in the initial amorphous matrix and the 0% level the Nb concentration in the α-FeCo nanocrystals.

3.2. Cu effect on the second crystallization process

The crystalline volume fraction at the end of the nanocrystallization process is independent of Cu addition for the studied alloys, being the same for 18 and 39 at.% Co-containing alloys ($\sim$55%) and smaller for the 60 at.% Co alloys ($\sim$45%). This fact has been explained in terms of an exhausted amorphous matrix in Fe concentration for the highest Co-containing alloys [22].

For a similar crystalline volume fraction, a larger average grain size implies that the average distance between the surfaces of neighbour nanocrystals becomes larger. Nb concentration, due to its low diffusivity, is supposed to be higher close to the nanocrystal surfaces than at the middle of the amorphous matrix [23]. Figure 5 schematically shows the effect of the thickness of the amorphous layer between nanocrystals on the Nb concentration profile: as the nanocrystals become closer, Nb concentration becomes more homogeneous.

This feature affects the second crystallization process. In fact, for a thicker amorphous layer, Nb concentration at the middle of this amorphous layer is lower and, therefore, the crystallization temperature of the residual amorphous phase might be lowered for this microstructure. (As known, crystallization temperature decreases as the Nb content decreases [24].) This hypothesis is verified in the studied alloys. In fact, for alloys with 18 and 39 at.% Co, addition of Cu decreases the grain size whereas crystalline volume fraction remains without significative change. Consequently, the amorphous layer between nanocrystals must be larger in the Cu-free alloys and, therefore, the crystallization temperatures might be lower in these alloys with respect to the corresponding Cu-containing alloys. On the other hand, for 60 at.% Co alloys, no significant difference in the microstructure can be observed and, consequently, no shift for the second crystallization process is expected. Figure 6 shows DSC scans for the temperature range of the second crystallization process. The results are in complete agreement with the proposed hypothesis on the effect of non-homogeneous Nb distribution in the residual amorphous matrix. As a consequence, a more refined microstructure yields to a stabilization of the nanocrystalline microstructure, shifting the second transformation stage to higher temperatures.

No difference can be appreciated between the second transformation enthalpies of two alloys with the same Co content. However, for the alloys with 18 and 39 at.% Co, the second transformation peak is broader for Cu-free alloys than for Cu-containing alloys. This fact is coherent with a more inhomogeneous Nb concentration in the amorphous matrix of Cu-free alloys due to their thicker amorphous layer between neighbour nanocrystals (figure 5). However, in 60 at.% Co alloys the transformation peak is broader for the alloy with Cu; in this case, no difference in the thickness of the amorphous layer is expected, but Cu cluster formed at earlier stages could provoke inhomogeneities in the residual amorphous matrix.

3.3. Cu effect on the magnetic properties

As indicated above, improvement of magnetic properties is an important target in the study of Hitperm alloys. Therefore, it is important to study the effect of the different microstructure

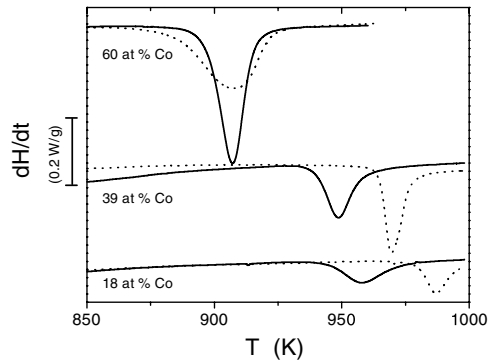

Figure 6. DSC scans at 10 K min^{-1} for the second transformation stage temperature range. Dotted curves correspond to alloys with Cu and solid curves to Cu-free alloys.

induced by the addition of Cu on the magnetic properties of these alloys. This would not only give a clearer picture of the relationship between microstructure and magnetic properties, but would also help in looking for new materials with improved magnetic properties.

In a previous work [25], a clear effect of the addition of Cu on magnetostriction was reported. For Cu-containing alloys, a maximum in the saturation magnetostriction constant (λ_S) was detected just before nanocrystallization onset, unlike for Cu-free alloys, in which a constant value of λ_S is observed before nanocrystallization. This feature was ascribed to the Cu cluster formation.

Figure 7 shows coercive field evolution with the temperature of heat treatment (T_a) for the different studied alloys (heated up to T_a at a constant heating rate of 10 K min^{-1}). The effect of different microstructures might affect the behaviour after nanocrystallization (temperature range between arrows in figure 7). The differences observed at lower temperatures are due to the structural relaxation process and domain wall stabilization [25], and will not be discussed here.

Cu addition induces significant differences in coercivity only between the alloys with 18 at.% Co content, with larger values for the alloy without Cu. This is in agreement with the larger grain size observed for the alloy without Cu (∼20 nm) with respect to the alloy with Cu (∼5 nm). For the other alloys, no remarkable differences are observed, indicating that grain size differences are not large enough (in the case of the alloys with 39% at Co, with ∼5 and 7.5 nm for the alloys with and without Cu, respectively). Therefore, other effects common for Cu-containing and Cu-free alloys are more important, such as the magnetoelastic anisotropy, associated with the large magnetostriction exhibited by these alloys [25].

In the following, a detailed study of the influence of Cu addition on the evolution of coercivity with crystalline volume fraction will be made for the 18 at.% Co-containing alloys. Both alloys exhibit the same composition of the nanocrystals and a similar crystalline volume fraction at the end of the nanocrystallization, the main difference being the grain size. For similar crystalline volume fractions the coercivity ratio between both alloys is $H_c(\text{Cu free})/H_c(\text{Cu}) < 5$. This value cannot be apparently justified if we assume a potential dependence of coercivity with the grain size (a D^6 law [16] would give ratios of ∼4096 and a D^3 law [26] ratios of ∼64).

Hernando *et al* [17] described the behaviour of magnetic anisotropy (k_{eff}) as a function of the crystalline fraction (x) as

$$k_{eff} = \frac{k_0 x}{\gamma^3} + \frac{3}{2}\lambda_S \sigma \tag{1}$$

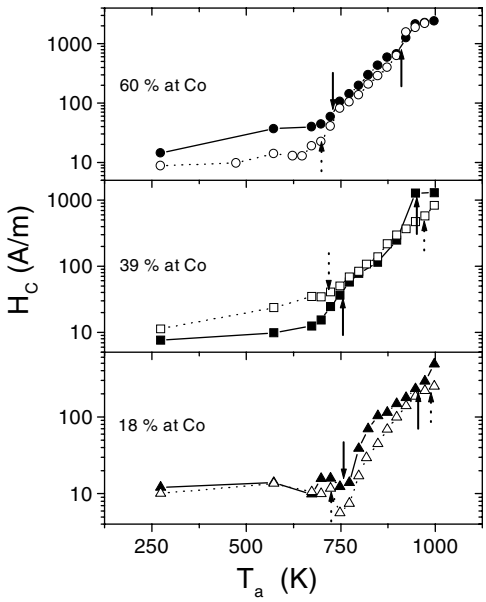

Figure 7. Coercive field versus temperature of heat treatment (heated up to T_a at 10 K min^{-1}). Dotted curves and white symbols correspond to alloys with Cu; solid curves and black symbols correspond to alloys without Cu. Arrows indicate the crystallization temperatures for the different transformation stages (dotted arrows, Cu-containing alloys; solid arrows, Cu-free alloys).

where $0 < \gamma < 1$ is the ability of the matrix to transmit the exchange coupling between the nanocrystals, dependent on x, λ_S is the saturation magnetostriction constant, σ is the internal stress and k_0 is the average magnetocrystalline anisotropy, which is related to the grain diameter (D) by

$$k_0 = \left(\frac{3}{4}\right)^3 \frac{D^6 k^4}{A^3} \tag{2}$$

where k is the magnetocrystalline anisotropy of the α-FeCo phase and A is the exchange stiffness.

Finally, coercivity can be approximated to

$$H_C \approx \frac{k_{eff}}{2\mu_0 M_S}. \tag{3}$$

The saturation magnetization (M_S) also depends on the crystalline volume fraction through the proportion of the different phases contributing to the total magnetization of the sample:

$$M_S = M_{Am}(1 - x) + M_{Cr}x \tag{4}$$

where M_{Am} and M_{Cr} are the saturation magnetization for the amorphous and crystalline phases, respectively. Whereas the composition of the nanocrystals is constant and, consequently, $\mu_0 M_{Cr}$ can be considered independent of x (2.4 T at 0 K [27], which corresponds to 2.16 T at 300 K), the amorphous phase is enriched in Nb and B [14] and a decrease of M_{Am}, as the crystallization progresses, can be expected. The atomic composition of the amorphous matrix in B and Nb can be easily calculated assuming 0% of B and Nb inside the nanocrystals:

$$C_{Am} = C_{In}/(1 - x) \tag{5}$$

where C_{In} is the B plus Nb content in the initial amorphous matrix (22 and 21 at.% for Cu-free and Cu-containing alloys, respectively). In this formula, the difference between crystalline

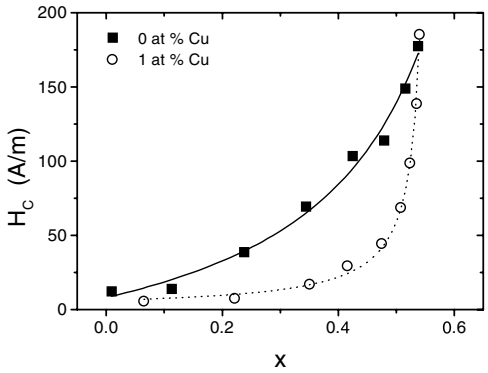

Figure 8. Coercivity versus crystalline volume fraction. Curves correspond to the fitting curve $y = (1 + cx)/(a + bx)$, values shown in table 1.

volume fraction (x) and crystalline atomic fraction (A_C), with ratios of $x/A_C = 1.14$ [28], has been neglected to simplify the following expressions. As a simple estimation, a constant decrease of the magnetization with the atomic per cent (p) enrichment of B and Nb will be assumed. This makes it possible to write

$$M_{Am} = M^0_{Am}\left(1 - p\left(\frac{C_{In}}{1-x} - C_{In}\right)\right) = M^0_{Am}\left(1 - \frac{Px}{1-x}\right) \tag{6}$$

with $P = pC_{In}$. Therefore, M_S can be calculated from (4) and (6) as

$$M_S = M^0_{Am} + (M_{Cr} - (1+P)M^0_{Am})x. \tag{7}$$

From (3) and (7), the evolution of coercivity could be fitted to a function of the form

$$H_C \approx \frac{1+cx}{a+bx} \tag{8}$$

where

$$a = \frac{2\mu_0 M^0_{Am}}{\frac{3}{2}\lambda_S\sigma} = \frac{2\mu_0 M^0_{Am}}{k_u}, \tag{9a}$$

$$b = \frac{2\mu_0(M_{Cr} - (1+P)M^0_{Am})}{k_u} \tag{9b}$$

and

$$c = \frac{k_0}{k_u}. \tag{9c}$$

It is important to note that γ has been approximated to unity (which would not be a strong restriction for small crystalline size, high crystalline volume fraction, low internal stresses or if the magnetoelastic contribution in equation (1) dominates over the other [17]) and $k_u = (3/2)\lambda_S\sigma$ has been considered to be independent of x. However, for the alloys with 18 at.% Co content, λ_S is similar for amorphous and nanocrystalline samples [25] and, therefore, the assumption is reduced to neglect the changes in σ for these alloys.

Figure 8 shows the fitting plots for both alloys with 18 at.% Co, with and without Cu, and table 1 presents the values obtained along with the experimental results used. Values of the crystalline volume fraction were obtained from the increase in magnetization with the nanocrystallization detected by thermogravimetry, at 10 K min^{-1} [21], correcting the dependence of the specific magnetization on the temperature. From the constant composition

Table 1. Parameters obtained by fitting the coercivity values versus crystalline volume fraction using the $y = (1 + cx)/(a + bx)$ function. Values obtained experimentally as well as literature values necessary to obtain the relevant information are also included. VSM, vibrating sample magnetometer; SAMR, small-angle magnetization rotation.

	$Fe_{60}Co_{18}Nb_6B_{15}Cu_1$	$Fe_{60}Co_{18}Nb_6B_{16}$	From
a	0.160	0.122	Fitting
b	−0.286	−0.159	Fitting
c	0.004	9.74	Fitting
$\mu_0 M^0_{Am}$ (T)	1.1	1.2	Experimental (VSM)
$\mu_0 M_{Cr}$ (T)	2.4(0 K) → 2.16(300 K)		[27]
D (nm)	5	20	Experimental (TEM)
λ_S (ppm)	16	13	Experimental (SAMR)
k_u (J m^{-3})	14	20	Fitting
σ (MPa)	0.6	1.0	Fitting
P	2.8	2.1	Fitting
k_0 (J m^{-3})	0.055	190	Fitting
A (J m^{-1})	10^{-11}		[32]
k (J m^{-3})	9600	9200	Fitting
	$\sim 10^4$		[32]

of the nanocrystals [14], a Curie temperature of 1203 K [29] has been assumed to describe the evolution of the specific magnetization. A good agreement is obtained between experiments and the model. The different grain size is the main factor responsible for the different quantitative behaviour of coercivity. For Cu-containing alloy average magnetocrystalline anisotropy (0.055 J m^{-3}) could be neglected with respect to magnetoelastic anisotropy (14 J m^{-3}), whereas for Cu-free alloy average magnetocrystalline anisotropy (190 J m^{-3}) is even one order of magnitude larger than the magnetoelastic anisotropy (20 J m^{-3}). In both cases, non-averaged magnetocrystalline anisotropy is $\sim 10^4$ J m^{-3}. As expected from the value of the critical grain size, $D_0 = (A/k)^{0.5} \sim 32$ nm (larger than the grain size in both alloys), nanocrystals are magnetically coupled in both alloys.

Internal stresses and parameter P present values of the same order for both alloys. The former, σ, shows similar values to that found for structurally relaxed amorphous samples ($\sim$1 MPa) [30, 31]. The latter gives a decrease $\sim$ 0.1% per Nb + B atom enrichment of the amorphous matrix, which is of the same order as the 0.05% per Nb atom enrichment in FeBNb amorphous alloys [24].

For the alloys with 39 and 60 at.% Co, the continuous increase of the saturation magnetostriction as nanocrystallization progresses [25] prevents the application of the previously described method. It has been previously shown that the most important compositional dependence of coercivity is the Co content of the alloy, due to its influence on magnetostriction, while Cu addition has a minor influence on coercivity.

4. Conclusions

The effect of Cu addition on microstructure, crystallization process and coercivity has been studied for an alloy series of Nb-containing Hitperm-type alloys with different Co contents.

Cu addition clearly refines the microstructure in the alloys with the lowest Co content but the effect is reduced as the Co content increases, disappearing for the 60 at.% Co alloys. This fact can be understood in terms of an enhancement of the nucleation process due to the Cu cluster formation in the alloys with Cu, and a larger impingement of the grain growth as the Co content increases in the alloy.

Microstructure affects the second crystallization process through the Nb concentration profile in the residual amorphous matrix. A more refined microstructure stabilizes the nanocrystalline microstructure, shifting the second crystallization process to higher temperatures.

The effect of Cu addition on magnetic properties is clearly observed for the alloys with lowest Co content, in which Cu addition has the strongest effect on the microstructure, reducing the average grain size from ∼20 to 5 nm. A fitting procedure of coercivity versus crystalline volume fraction is performed for these alloys assuming constant magnetoelastic anisotropy. Microstructure differences cannot explain the differences found in coercivity between alloys with different Co contents, which must be explained in terms of the different magnetostriction evolution as the nanocrystallization progresses.

Acknowledgments

This work was supported by the Spanish Government and EU FEDER (project MAT 2001-3175) and the PAI of the Junta de Andalucía. J S Blázquez acknowledges a research fellowship of the DGES.

References

[1] Yoshizawa Y, Oguma S and Yamauchi K 1988 *J. Appl. Phys.* **64** 6044
[2] Yoshizawa Y and Yamauchi K 1990 *Mater. Trans. JIM* **21** 307
[3] Suzuki K, Makino A, Kataoka N, Inoue A and Masumoto T 1991 *Mater. Trans. JIM* **32** 93
[4] Suzuki K, Makino A, Inoue A and Masumoto T 1991 *J. Appl. Phys.* **70** 6232
[5] Willard M A, Laughlin D E, McHenry M E, Thoma D, Sickafus K, Cross J O and Harris V G 1998 *J. Appl. Phys.* **84** 6773
[6] Zhang Y, Hono K, Inoue A and Sakurai T 1996 *Mater. Sci. Eng.* A **217/218** 407
[7] Hono K, Ping D H, Ohnuma M and Onodera H 1999 *Acta Mater.* **47** 997
[8] Ayers J D, Sprague V G and Elam W T 1994 *Appl. Phys. Lett.* **64** 974
[9] Ayers J D, Sprague V G, Elam W T and Jones H N 1998 *Acta Mater.* **46** 1861
[10] Borrego J M, Conde C F, Conde A, Chadwick A V and Morrison G 1998 *J. Non-Cryst. Solids* **232–234** 352
[11] Swilem Y, Sobczak E, Nietubyc R, Slawska-Waniewska A and Tischer M 1998 *J. Non-Cryst. Solids* **232–234** 665
[12] Hono K 2002 *Advanced Magnetic Materials: Characterisation and Simulation of Advanced Magnetic Materials* ed Y Liu, D J Sellmyer, D Shindo, J G Zhu and G C Hadjipanayis (Berlin: Springer) at press
[13] Ping D H, Wu Y Q, Hono K, Willard M A, McHenry M E and Laughlin D E 2001 *Scr. Mater.* **45** 781
[14] Zhang Y, Blázquez J S, Conde A, Warren P J and Cerezo A 2002 *Mater. Sci. Eng.* A at press
[15] McHenry M E, Willard M A and Laughlin D E 1999 *Prog. Mater. Sci.* **44** 291
[16] Herzer G 1989 *IEEE Trans. Magn.* **25** 332
[17] Hernando A, Vázquez M, Kulik T and Prados C 1995 *Phys. Rev.* B **51** 3581
[18] Franco V, Ramos-Martos J and Conde A 1996 *Rev. Sci. Instrum.* **67** 4167
[19] Blázquez J S, Conde C F and Conde A 2001 *J. Non-Cryst. Solids* **287** 187
[20] Okhubo T, Kai H, Ping D H, Hono K and Hirotsu Y 2001 *Scr. Mater.* **44** 971
[21] Blázquez J S, Conde C F and Conde A 2002 *Appl. Phys.* A at press
[22] Blázquez J S, Franco V, Conde C F and Conde A 2002 *J. Magn. Magn. Mater.* at press
[23] Yavari A R and Drbohlav O 1995 *Mater. Trans. JIM* **36** 896
[24] Wijn H P J 1991 *Landolt–Börnstein: Magnetische Eigenschafen von Metallen* (Berlin: Springer)
[25] Blázquez J S, Franco V, Conde A, Gibbs M R J, Davies H A and Wang Z C 2002 *J. Magn. Magn. Mater.* **250** 260
[26] Suzuki K, Herzer G and Cadogan J M 1998 *J. Magn. Magn. Mater.* **177–181** 949
[27] Bozorth R M 1968 *Ferromagnetism* (Princeton, NJ: Van Nostrand-Reinhold)
[28] Blázquez J S, Conde A and Grenèche J M 2002 *Appl. Phys. Lett.* **81** 1612
[29] Fernández-Guillermet A 1987 *High Temp.–High Pressures* **19** 477
[30] Blázquez J S, Franco V, Conde A and Kiss L F *J. Magn. Magn. Mater.* submitted
[31] Gutiérrez J, Muto V and Squire P T 2001 *J. Non-Cryst. Solids* **287** 417
[32] O'Handley R C 1999 *Modern Magnetic Materials: Principles and Applications* (New York: Wiley)